REPORT DOCUMENTATION PAGE

Form Approved
OMB NO. 0704-0188

Public Reporting burden for this collection of information is estimated to average 1 hour per response, including the time for reviewing instructions, searching existing data sources, gathering and maintaining the data needed, and completing and reviewing the collection of information. Send comment regarding this burden estimates or any other aspect of this collection of information, including suggestions for reducing this burden, to Washington Headquarters Services, Directorate for information Operations and Reports, 1215 Jefferson Davis Highway, Suite 1204, Arlington, VA 22202-4302, and to the Office of Management and Budget, Paperwork Reduction Project (0704-0188,) Washington, DC 20503.

1. AGENCY USE ONLY (Leave Blank)	2. REPORT DATE 26 Nov 2003	3. REPORT TYPE AND DATES COVERED Final Technical 15Aug1999-31Dec2001

4. TITLE AND SUBTITLE

High Power Mid-IR Semiconductor Lasers for LADAR

5. FUNDING NUMBERS
N00014-99-1-1023

6. AUTHOR(S)

Luke Lester

7. PERFORMING ORGANIZATION NAME(S) AND ADDRESS(ES)
The University of New Mexico
Center for High Technology Materials,
1313 Goddard SE (MSC04 2710)
Albuquerque, NM 87106

8. PERFORMING ORGANIZATION REPORT NUMBER

310571FT

9. SPONSORING / MONITORING AGENCY NAME(S) AND ADDRESS(ES)

Office of Naval Research
Ballston Centre Tower One
800 North Quincy Street
Arlington, VA 22217-5660

10. SPONSORING / MONITORING AGENCY REPORT NUMBER

11. SUPPLEMENTARY NOTES
The views, opinions and/or findings contained in this report are those of the author(s) and should not be construed as an official Office of Naval Research position, policy or decision, unless so designated by other documentation.

12 a. DISTRIBUTION / AVAILABILITY STATEMENT

Approved for public release; distribution unlimited.

12 b. DISTRIBUTION CODE

13. ABSTRACT (Maximum 200 words)

The growing need for antimonide-based, room temperature, 2-5 μm, semiconductor lasers for trace gas spectroscopy, ultra-low loss communication, infrared countermeasures, and ladar motivated this work. To extend the wavelength of semiconductor lasers beyond 2 μm, increased arsenic content has been needed to reduce the bandgap and maintain a lattice match to GaSb. This has resulted in degraded performance due in part to a smaller valence band offset. In this work, the need for lattice match between the active region and the GaSb substrate is avoided by the use of metamorphic AlInSb buffer layers. This provides a virtual substrate to extend the wavelength of GaInSb quantum wells. With the use of lattice constants larger than GaSb, the need for arsenic has been eliminated resulting in pure antimonide crystals, which provides for large valence band offsets.

Samples are grown by solid source molecular beam epitaxy. The AlInSb metamorphic buffer layer is a superlattice consisting of alternating layers of $Al_xIn_{1-x}Sb$ and $Al_yIn_{1-y}Sb$ where the indium content and thickness ratios are chosen to provide the desired average indium content. Using these buffer layers, optically pumped GaInSb/AlGaInSb multiple quantum well lasers with as much as 76% indium content in the quantum well and emission wavelength as long as 3.3 μm at room temperature have been achieved. The best performing room temperature laser emits at 2.8 μm with a threshold power density of 169 W/cm2 and a differential quantum efficiency of 28%.

14. SUBJECT TERMS
Semiconductor Lasers, GaInSb Quantum Wells

15. NUMBER OF PAGES

17

16. PRICE CODE
NSP

17. SECURITY CLASSIFICATION OR REPORT UNCLASSIFIED	18. SECURITY CLASSIFICATION ON THIS PAGE UNCLASSIFIED	19. SECURITY CLASSIFICATION OF ABSTRACT UNCLASSIFIED	20. LIMITATION OF ABSTRACT UL

NSN 7540-01-280-5500

Standard Form 298 (Rev.2-89)
Prescribed by ANSI Std. 239-18
298-102

20031217 258

FINAL TECHNICAL REPORT

to

OFFICE OF NAVAL RESEARCH

GRANT # N00014-99-1-1023

for the period

15 Aug 1999 - 31 Dec 2001

entitled

"High Power Mid-IR Semiconductor Lasers for LADAR"

by

Professor Luke F. Lester

University of New Mexico

Center for High Technology Materials

Technical Summary

The growing need for antimonide-based, room temperature, 2-5 μm, semiconductor lasers for trace gas spectroscopy, ultra-low loss communication, infrared countermeasures, and ladar motivated this work. To extend the wavelength of semiconductor lasers beyond 2 μm, increased arsenic content has been needed to reduce the bandgap and maintain a lattice match to GaSb. This has resulted in degraded performance due in part to a smaller valence band offset. In this work, the need for lattice match between the active region and the GaSb substrate is avoided by the use of metamorphic AlInSb buffer layers. This provides a virtual substrate to extend the wavelength of GaInSb quantum wells. With the use of lattice constants larger than GaSb, the need for arsenic has been eliminated resulting in pure antimonide crystals, which provides for large valence band offsets.

Samples are grown by solid source molecular beam epitaxy. The AlInSb metamorphic buffer layer is a superlattice consisting of alternating layers of $Al_xIn_{1-x}Sb$ and $Al_yIn_{1-y}Sb$ where the indium content and thickness ratios are chosen to provide the desired average indium content. Using these buffer layers, optically pumped GaInSb/AlGaInSb multiple quantum well lasers with as much as 76% indium content in the quantum well and emission wavelength as long as 3.3 μm at room temperature have been achieved. The best performing room temperature laser emits at 2.8 μm with a threshold power density of 169 W/cm^2 and a differential quantum efficiency of 28%.
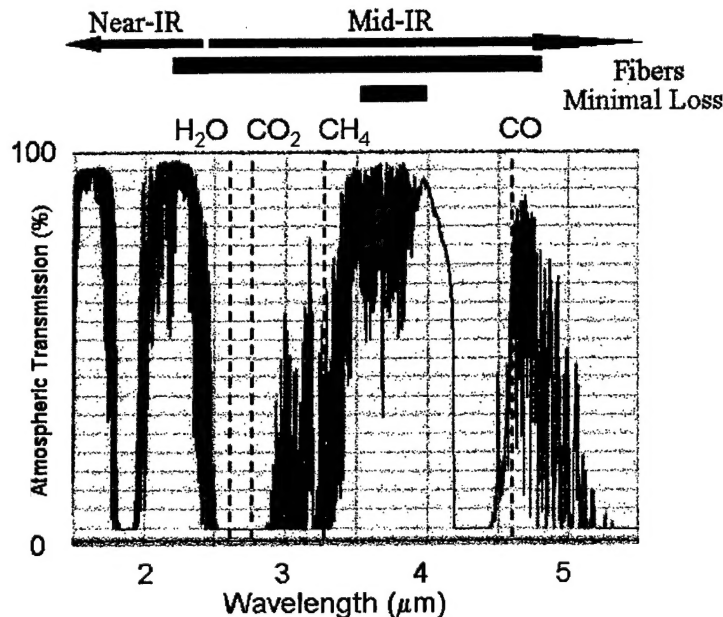
Final Technical Report

Figure 1 Infrared transmission through the atmosphere showing possible applications.[1]

Mid-infrared (2.5-10 μm) lasers have application in ultra-low loss fiber communications[2], trace-gas detection[3], and atmospheric transmission including ladar[4], communication, and countermeasures. Mid-infrared (IR) fluoride and chalcogenide glass fibers have several orders of magnitude less loss than near-IR (0.7-2.5 μm) fibers reducing the power needed. Absorption by trace gas detection is several orders of magnitude stronger in the mid-IR than in the near-IR. Some of the more common gases that absorb in the mid-infrared region are water vapor, carbon dioxide, carbon monoxide and methane. These exhibit strong absorption at 2.63 μm, 2.78 μm, 4.60 μm and 3.28 μm, respectively. Also, a variety of applications like free-space communication and countermeasures exist near 3.8 μm where atmospheric losses are least. These wavelengths are depicted in Figure 1, which shows infrared transmission through the atmosphere. For these various applications, mid-IR semiconductor lasers are generally preferred over other possible solid-state sources because of their compact size, low weight, watt-level powers, and reasonable beam divergence.

3

Many different semiconductor solutions have been proposed and researched in the past decade to improve the performance of mid-IR lasers, but the challenge to reduce the cooling requirements in these devices still remains. No particular engineering design for mid-IR laser sources dominates because each one makes tradeoffs of one sort or another. Thus, intersubband quantum cascade (QC), interband quantum cascade, "W" lasers, type-I heterojunction, type-II heterojunction, and double heterostructure lasers all compete in the mid-IR arena. The advantages, limitations, and complexities of several of these laser types will be described later in this chapter, and the motivation for the ground-breaking GaInSb/AlGaInSb type-I design discussed in this thesis will become apparent. The precept of this work is that simplicity in crystal growth and laser design will ultimately yield a robust, reproducible and understandable design. We show that the new type of pure antimonide laser that is proposed and studied in this work allows for room temperature operation at longer wavelengths, which reduces the cooling requirements of the device.

Tradeoffs in Current Mid-IR Semiconductor Lasers

	Type-I QW	Baranov QW	'W' QW	Intersubband QC	Interband QC
Growth	Simple	Simple	Complex	Very Complex	Very Complex
Injection	Excellent	Poor	Poor	Good	Good
CW	Good	Good	Good	Poor	Poor
Threshold	Small	Fair	Fair	Large	Fair
2-5 μm	Poor	Fair	Good	Poor (LWIR)	Good

Table 1 Summary of tradeoffs of mid-IR semiconductor lasers. Type-I QW, Baranov QW, 'W' QW, intersubband quantum cascade and interband quantum cascade are included in the table. The listed factors include growth complexity, electrical-injection characteristics, CW characteristics, threshold densities, and 2-5 μm coverage.

In order to push the performance envelope, the trend has been toward more and more complex structures that become increasing difficult to grow. A summary of the tradeoffs for mid-IR semiconductor lasers is given in Table 1. The vast majority of commercial semiconductor lasers are type-I QWs. This is due to their simplicity and high performance. However, this is limited to near-IR emission wavelengths. Mid-IR emission has been complicated by poor valence band offsets, limited emission wavelengths and materials that are difficult to grow. Baranov style QW lasers eliminate the limitation on emission wavelength but they exhibit greatly reduced gains and differential gains along with poor electrical injection characteristics at mid-IR wavelengths. 'W' QW lasers have increased gain and differential gain over Baranov style lasers but fall short of type-I expectations. Also, the poor electrical characteristics of type-II structures remain. Intersubband quantum cascade lasers exhibit long wavelengths, but they have large threshold current densities and perform well only when operated pulsed. Interband

quantum cascade lasers exhibit shorter wavelengths and lower threshold current densities than the intersubband versions, but the problem with heat sinking remains.

The Pure Antimonide Solution

Mid-IR semiconductor lasers exhibit a trend to more complex structures to achieve the desired performance characteristics. However, increased performance for the simplest type-I QW lasers can be achieved in the mid-IR region. This goal is achieved by eliminating InAs from the growth and using the GaInSb/AlGaInSb material system. This removes the deleterious type-II valence band alignment of InAs and allows for simpler pure antimonide growths. If only GaSb or InAs substrates are employed, the emission is limited to near-IR wavelengths. In order to get around this limitation, it is necessary to grow on larger lattice constant substrates, which will allow for longer mid-IR wavelengths by having larger InSb content in the QW. However, there are no available substrates with lattice constants between GaSb and InSb. In order to achieve larger lattice constants, it is necessary to grow the laser structure on relaxed buffer layers such as AlInSb on GaSb substrates. Such relaxed layers are referred to as metamorphic buffers.

Some pure antimonide lasers have been previously reported. Double heterostructure (DH) AlGaSb/GaSb lasers grown on GaSb have been reported with room temperature emission at 1.78 μm.[5] InSb homostructure lasers have been reported operating at 2K with emission at 5.22 μm.[6] The growth of DH laser with InSb can not be achieved due to all alloys with InSb having a large tensile strain on InSb substrates. However, strained InAlSb/InSb heterostructure lasers grown on InSb have been reported emitting at 5.1 μm at 90K where doping provides the cladding and the InAlSb barrier helps confine the carriers for these devices, but the amount of alloyed aluminum and thickness of InAlSb on InSb substrates is greatly limited resulting in poor optical and carrier confinement.[7]

Larger differential gains are expected for GaInSb/AlGaInSb pure antimonide type-I quantum wells when compared with mixed arsenic and antimony type-I QWs due to larger possible valence band offsets at longer wavelengths. However, the nature of metamorphic buffers is to produce dislocations. This will result in increased SRH recombination and optical scattering. Enough of the dislocations must be prevented from threading into the active region to demonstrate the usefulness of any improved pure antimonide laser. This challenge is met using strained AlInSb superlattice metamorphic buffer layers, where the superlattice is used to filter dislocations. Larger InSb content results in larger lattice constants and longer emission wavelengths. However, the metamorphic buffer's ability to trap threading dislocations limits the InSb content.

Thus, high performance laser structures are sought by growing GaInSb/AlGaInSb quantum wells. The resulting structures are completely free from arsenic leading to pure antimonide laser structures. The consequences of having only one group-V element are of particular importance to the grower where mixed group-V's greatly complicate growth. The As/Sb ratio is difficult to maintain where each epitaxial layer must be repeatedly calibrated. Many compositions will phase separate due to the substantial miscibility gaps in mixed As/Sb alloys. Also, the arsenic for antimony exchange and interfacial bond type further complicate growth.

Metamorphic Buffers

All the MQW lasers grown in this study are pure antimonides. Virtual substrates are grown on (100) undoped GaSb composed of metamorphic AlInSb epilayers step-graded with dislocation filtering. The large valence band offsets (greater than 75 meV) are achieved with GaInSb/AlGaInSb. Samples were grown by solid-source molecular beam epitaxy (MBE) on a Vacuum Generators V80H with an Applied Epi-Veeco valved antimony cracker. The available group III effusion cells are one gallium, two aluminum and two indium cells.
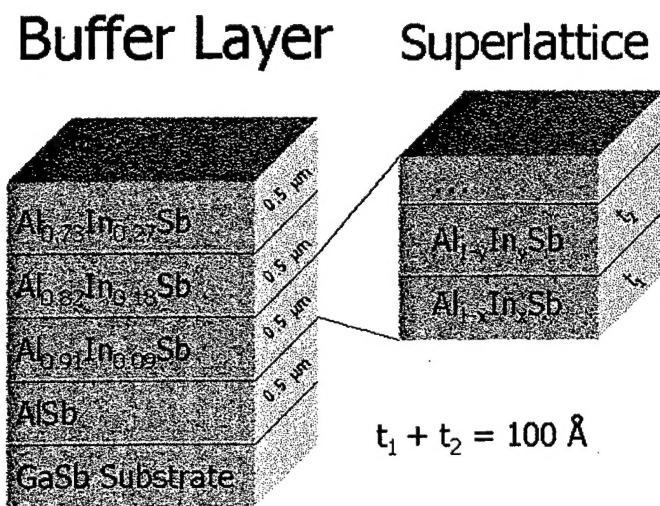
Figure 2 Schematic for an AlInSb metamorphic buffer with a superlattice filter.

Figure 2 shows a schematic for the metamorphic buffer. It is composed of 0.5 μm thick step-graded layers whose average composition is $Al_{1-s}In_sSb$ where the average indium content, s, is increased in 9% steps. Continuously graded buffers are marginally smoother, but steps larger than 9% result in extremely rough surfaces. This is possibly due to the change in growth mode from Frank-Van der Merwe to Volmer Weber. The buffers will subsequently be named by the final buffer layer or the average indium content in the final buffer layer. Thus, the grown metamorphic buffers are 27% or $Al_{0.73}In_{0.27}Sb$, 36% or $Al_{0.64}In_{0.36}Sb$, 45% or $Al_{0.55}In_{0.45}Sb$ and 54% or $Al_{0.46}In_{0.54}Sb$ buffers corresponding to an average final layer composition of $Al_{0.73}In_{0.27}Sb$, $Al_{0.64}In_{0.36}Sb$, $Al_{0.55}In_{0.45}Sb$, and $Al_{0.46}In_{0.54}Sb$, respectively.

Samples were grown at 500 °C. The first step is AlSb and it is a 0.5 μm thick layer. This layer was sometimes grown at 520°C to decrease the surface roughness of the buffer. This is due to increased surface mobility of the atoms. This can be seen in the liquidous-solidous points of AlInSb where AlSb is 500 °C larger than InSb. Also, this demands reduced growth temperatures

6

for increased InSb content. The final step in the $Al_{0.46}In_{0.54}Sb$ metamorphic buffer and active regions on it required a reduced temperature of 480 °C.

The average composition of the stepped layer is formed from a binary superlattice dislocation filter, which is composed of a 100 Å period of $Al_{1-x}In_xSb/Al_{1-y}In_ySb$. AlSb, $Al_{0.7}In_{0.3}Sb$, $Al_{0.4}In_{0.6}Sb$ were used to produce the average compositions in most samples, which were grown between 0.75 monolayers/second and 1 monolayer/second depending on the epilayer. Slower growth rates of 0.5 monolayers/second decreased the roughness of the sample, but this substantially increases the growth time. Increased growth rates decrease surface mobility resulting in rougher surfaces. The total growth times are around 10 hrs for the complete laser structures. Improvements with the slower growth rates and thicker buffers can increase the total growth time beyond 20 hours. However, no buffer remains smooth beyond a 3% change in lattice constant. This corresponds to a buffer with a top layer composition of $Al_{0.58}In_{0.42}Sb$.

Results for Pure Antimonide Lasers

Freed from the constraint of substrate lattice constants, the design of pure antimonide type-I QW lasers has a few special considerations. The emission wavelength is increased by increasing the lattice constant using increased InSb content. The valence band offset is critical for proper carrier confinement, which must be at least 75 meV. However, the valence band offset is in competition with the optical confinement. In addition, high performance lasers result from large compressive strains in the QW. The limitation of strain on layer thickness and the effects of strain on design parameters must be considered. In order to understand all of these trends, a few basic models must be established.

The general design of the laser structure is given below. The quantum well active area for AlGaInSb/GaInSb type-I QW lasers is composed of AlGaInSb barriers lattice matched to the buffer with compressively strained GaInSb wells. The cladding shares the same composition as the terminating AlInSb buffer layer. The latter has the smallest index of refraction for this pure antimonide material system. Figure 3 shows a schematic diagram for the 0.5% strained MQW laser structure on the $Al_{0.64}In_{0.36}Sb$ buffer. It is composed of 2 μm $Al_{0.64}In_{0.36}Sb$ clads and a 1 μm thick core region of AlGaInSb. The 2 μm lower cladding was sometimes reduced by ½ μm where the last layer of the metamorphic buffer served as part of the lower cladding. The active region is composed of four 100Å $Ga_{0.5}In_{0.5}Sb$ quantum wells surrounded by $Al_{0.2}Ga_{0.4}In_{0.4}Sb$ barriers, which are used to separate the wells by 100 Å.

Al$_{0.64}$In$_{0.36}$Sb clad

100 Å Al$_{0.2}$Ga$_{0.4}$In$_{0.4}$Sb barriers

~80 meV

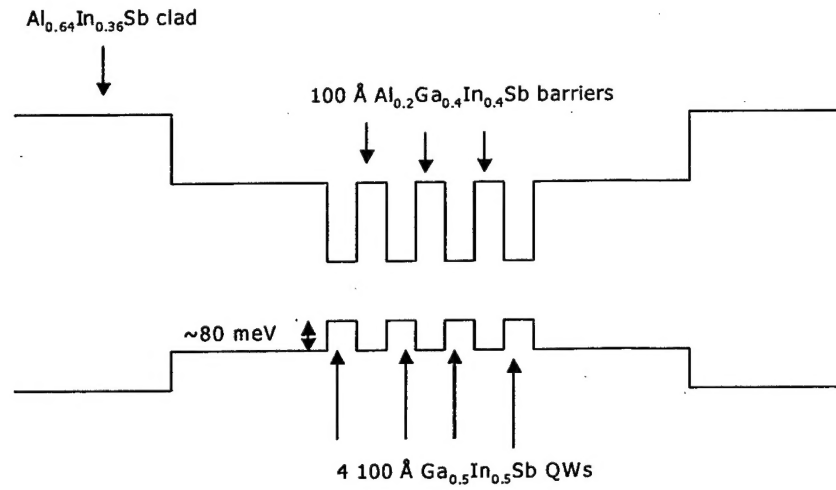4 100 Å Ga$_{0.5}$In$_{0.5}$Sb QWs

Figure 3 Schematic for the 0.5% strained quantum well laser structure on the 36% buffer.

Optically Pumped Laser Results

Sample	Clad Al$_{1-x}$In$_x$Sb	Barrier	QW Ga$_{1-x}$In$_x$Sb	% strain of QW	Emission wavelength (μm)@ max. temp. (K)
A	27%	Al$_{0.20}$Ga$_{0.48}$In$_{0.32}$Sb	42%	0.5	2.58@330
B	36%	Al$_{0.20}$Ga$_{0.40}$In$_{0.40}$Sb	50%	0.5	2.85@330
C	36%	Al$_{0.20}$Ga$_{0.40}$In$_{0.40}$Sb	60%	1.1	2.93@370
D	45%	Al$_{0.20}$Ga$_{0.31}$In$_{0.49}$Sb	60%	0.6	3.12@230
E	45%	Al$_{0.19}$Ga$_{0.32}$In$_{0.49}$Sb	68%	1.1	3.28@310
F	54%	Al$_{0.20}$Ga$_{0.23}$In$_{0.57}$Sb	76%	1.1	3.45@170

Table 2 The sample index with active area compositions. The maximum emission wavelength and operating temperature are included.

The substrates were lapped and polished to ~100 μm for lasers. Samples that are much thicker cleave poorly and samples that are much thinner are difficult to handle. The buffer itself did not appear to affect the quality of the cleave. The samples were cleaved into 1-mm cavities. The bars were mounted with indium epi-side up to copper heat sinks, and they were optically pumped on a cold finger in the custom cryostat. The 980 nm stacked diode array was focused into a 250 μm stripe for laser pumping. Power measurements were collected with a thermopile. 50 μs pulses are used for all testing. Power measurements are made using 5% duty cycle and all spectra were taken using a 50% duty cycle. The quantum deficit of the pump to the barriers at room temperature range from 0.56-0.45, and the quantum deficit from the barriers to the emission wavelength at room temperature range from 0.71-0.56. This is a total quantum deficit of 0.40-0.25.

The results are summarized in Table 2. The maximum wavelengths were achieved using a power on the order of a kW/cm^2. The emission wavelengths at the maximum temperatures are shown in the table. The MQW lasers on the 27% and 36% buffers all lased above room temperature, but the 1% compressively strain MQW laser on the 36% buffer lased to 370K with emission at 2.93 μm. The 0.6% compressively strained MQW laser on the 45% buffer would not lase at room temperature. It had a maximum operating temperature of 230K. By increasing the QW strain on this buffer, laser were fabricated that operated at room temperature at 3.28 μm. The samples on the 45% buffer showed decreased operating temperatures. Also, the uniformity across laser bars was decreased.

Samples on the 27% and 36% buffer lased nearly across the whole bars that were tested. This uniformity decreased on the 45% buffer lasers that have substantial regions with larger thresholds. The MQW laser on the 54% buffer did not lase across the majority of the bar at any temperature. It had a maximum operating temperature of 170K emitting at 3.45 μm. The spectrum of this sample at its maximum operating temperature is shown in Figure 4. The use of increased strain was used to increase the gain. This worked to increase the operating temperature on the 45% buffer to room temperature, but the expected increase in gain for larger strains does not appear to be substantial enough to increase the operating temperature on the 54% buffer to room temperature.
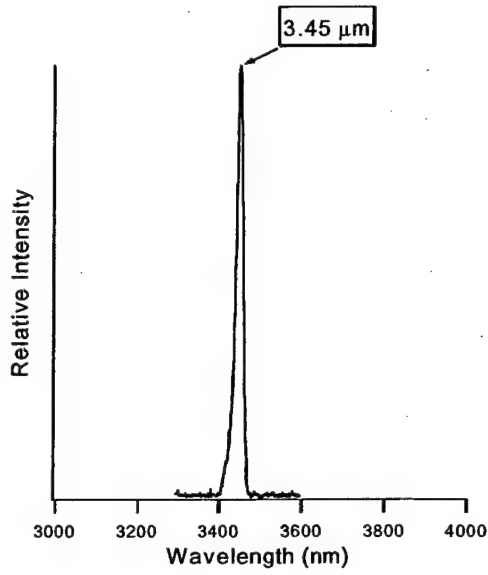
Figure 4 The 170K above-threshold spectra for sample F with the longest emission at 3.5 μm.
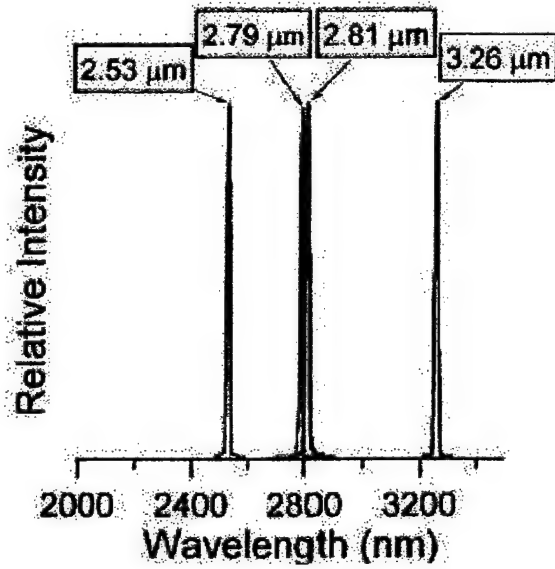

Figure 5 The 300K above-threshold spectra for samples A, B, C, and D.

Figure 5 shows the above threshold spectra of the 4 samples that lased at room temperature. Room temperature emission can be seen at 2.53 μm, 2.79 μm, 2.81 μm, and 3.26 μm from MQW lasers grown on 27%, 36%, 36%, and 45% buffers, respectively.
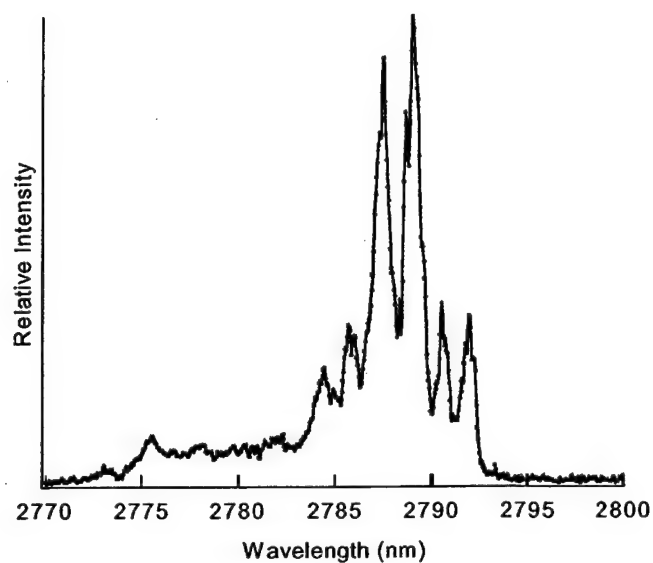
10

Figure 6 Above-threshold room-temperature spectrum for sample B expanded to reveal the multimode spectra.

The room temperature power curves for the MQW lasers with spectra in Figure 5 are shown in Figure 7. The 980 nm diode array was operated quasi-CW with pulse widths of 50 μs and a 5% duty cycle for this figure. Larger duty cycles increased thermal rollover but still showed the same thresholds and the same efficiency near threshold.
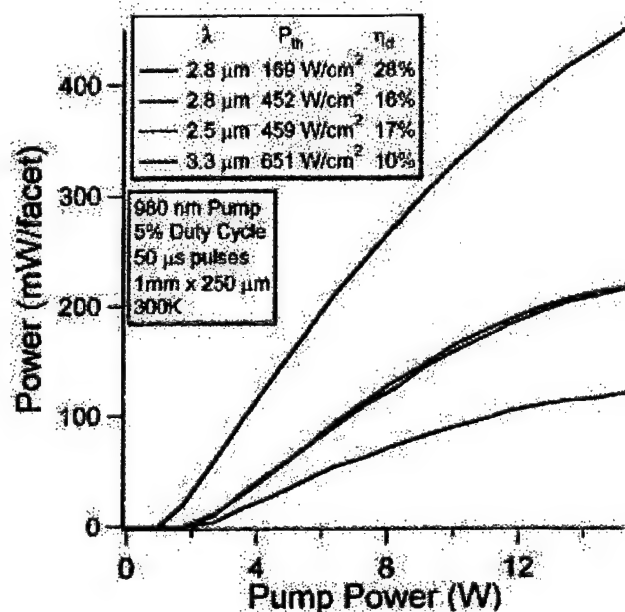
Figure 7 The pump power versus output power curve at 300K for samples A, B, C, and D.

The most power was emitted from the 1% compressively strained MQW laser on the 36% buffer which emitted 0.5 watt peak power per facet at room temperature. The 0.5% compressively strained MQW lasers on the 27% and 36% buffers showed identical performance. The laser on the 27% buffer is plotted in the figure. This shows about half the efficiency and twice the threshold of the 1% compressively strained MQW laser on the 36% buffer. Only the 1% compressively strained MQW laser on the 45% buffer lased at room temperature. It showed a reduced performance from the lasers grown on the 27% and 36% buffers.

A substantial reduction in threshold and increase in efficiency is seen between the 0.5% and 1% compressively strained MQW lasers on the 27% and 36% buffers. The 1% compressively strained MQW laser on the 36% buffer had a low threshold of 169 W/cm^2 at room temperature and a large differential quantum efficiency of 28%. Efficiencies were calculated assuming that 100% of the pump transmitted into the sample is absorbed. Long pass filters were used to block the 980 nm pump from the thermopile. The mirror and window losses were measured but the reflection from the samples surface was calculated to be 31% using indices of refraction from **Error! Reference source not found.**.

The low threshold densities and high quantum efficiencies are accompanied by large characteristic temperature indicating high performance lasers. The threshold current densities for the three samples characterized in the preceding figures between 200K and 300K is plotted in Figure 8. The characteristic temperature, T_0, is shown. The 0.5% compressively strained MQW lasers on the 27% and 36% buffers have a T_0 around 100K. This is substantially larger than other reported values. However, the 1% compressively strained MQW laser on the 36% buffer showed an even larger characteristic temperature of 119K, but the 1% compressive strained MQW laser on the 45% buffer showed a much lower T_0 of 76K. This indicates a degrading performance on the 45% buffer. Lasers on the 54% buffer would not lase at room temperature.
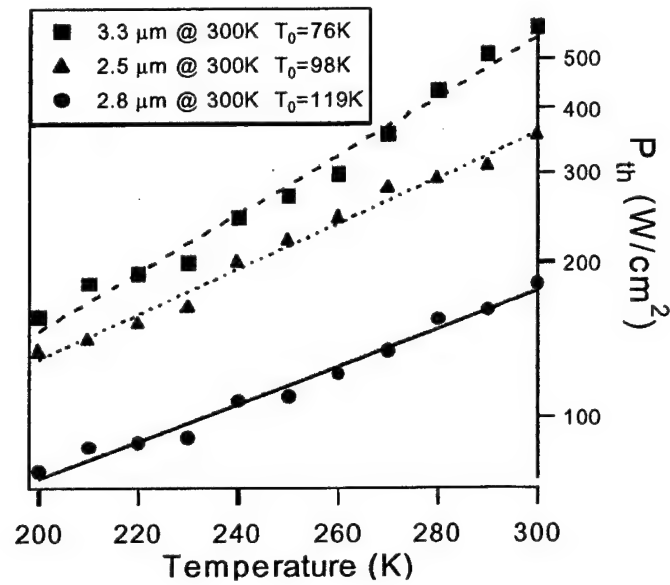
12

Figure 8 The characteristic threshold temperatures, T_0, between 200K and 300K for samples A, C, and D.
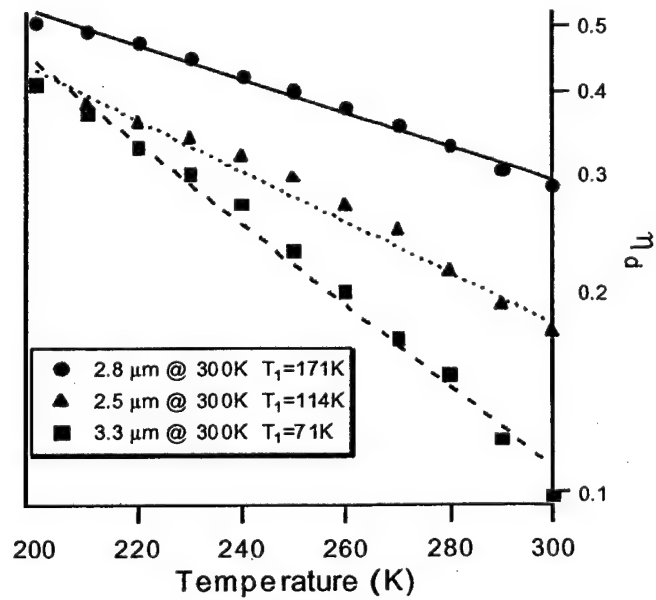

Figure 9 The characteristic efficiency temperatures, T_1, between 200K and 300K for samples A, C, and D.

The quantum efficiencies for the same three lasers between 200K and 300K are in Figure 9. The characteristic temperatures, T_1, are reported. The largest T_1 value is 171K for the 1%

compressively strained MQW laser on the 36% buffer. These characteristic temperatures are reported for temperatures that are achievable with thermoelectric cooling. However, across a wider range of temperature there is significant variation in the characteristic values between 100K and 350K.
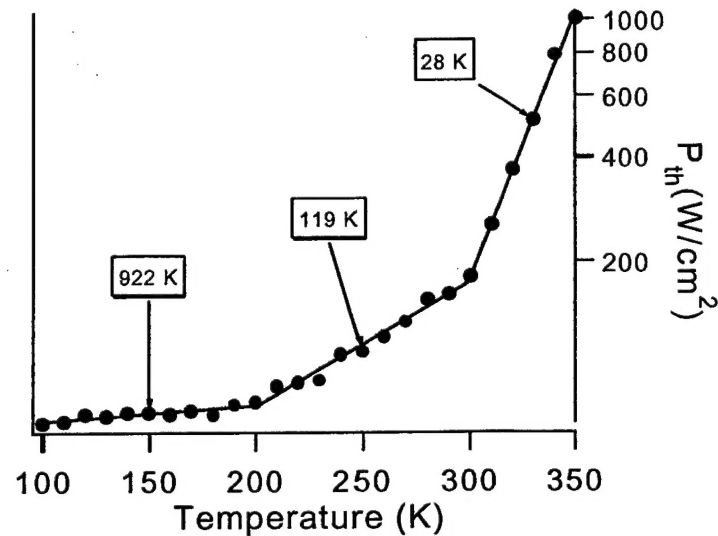

Figure 10 The characteristic threshold temperatures, T_0, between 100K and 350K for sample F. The performance shows three distinct regions where the T_0 ranged from 922K to 28K.

Figure 10 shows the T_0 characteristic temperature for the best performing sample, C, between 100K and 350K. Nevertheless the observed trends are representative of all lasers. All samples show distinct changes for both characteristic temperatures across the examined range. Below 200K at cryogenic temperatures, the thresholds and efficiencies are nearly constant. It would be expected that lasers with small defect densities should continue to have increasing efficiencies and decreasing thresholds below 200K. Therefore, the T_0 value of 922K between 100K and 200K for the best sample is indicative of a laser dominated by defects at low temperatures. Above room temperature, samples show much lower characteristic temperatures. A T_1 of 28K limits operation at extremely high temperatures. Auger rates may be contributing to these higher thresholds above 300K, but the dominant loss mechanism is SRH.

Conclusion

It is possible to create virtual substrates with lattice constants between AlSb and InSb by growing AlInSb metamorphic buffers on GaSb. The quality of these buffers is significantly degraded beyond a 3% change in lattice constant. This corresponds to an $Al_{0.58}In_{0.42}Sb$ buffer with a lattice constant of 6.279. The deleterious effect of these buffers is attributed defects due to the decrease in AlSb content. QW laser structures grown without AlSb superlattice layers show

14

reduced PL intensity. The AlSb/AlInSb superlattice acts as a filter preventing dislocations from threading into the active area. This is indicated by well ordered XRDs and TEMs.

PL taken from bulk $Ga_{1-x}In_xSb$ did not conform to the expected quadratic polynomial. Instead, a nonlinear bowing term is expressed that is weighted by the indium content for the ternary, GaInSb. This results in a cubic polynomial that provides a good fit to collected data. This deviation from expected models leaves an uncertainty in universally accepted band parameters. This is further complicated by reported discrepancies in strained material parameters. Nonetheless some rules of thumb and design trends for the AlGaInSb/GaInSb QW laser design have been given.
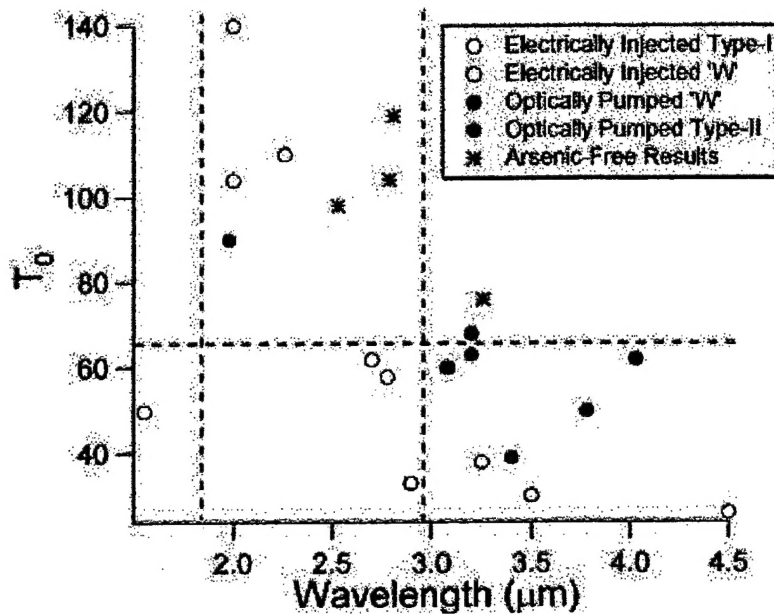

Figure 11 The characteristic threshold temperatures, T_0, of Type-I and Type-II quantum well structures between 2-4.5 μm. The arsenic-free lasers are included for comparison.

Arsenic-free, pure antimonide lasers grown on AlInSb metamorphic buffers showed improved performance over other type-I and type-II QW lasers with similar wavelengths. Figure 11 shows a comparison of T_0 values for mid-IR lasers. The degraded performance of typical arsenic-containing type-I QW lasers on GaSb is attributed to a loss of heavy-hole confinement resulting in lower differential gains. The improved valence band offsets for GaInSb/AlGaInSb remain roughly constant on various AlInSb metamorphic buffers maintaining heavy-hole confinement at longer wavelengths.

Lasers operated out to 3.3 μm at room temperature. Increased strain had a very large effect on the performance of GaInSb/AlGaInSb MQW lasers on AlInSb metamorphic buffers. The best performance was seen from 1% compressively strain MQW laser grown on the $Al_{0.64}In_{0.36}Sb$ buffer which emitted at 2.8 μm at 300K. It showed a differential quantum efficiency of 28% and a power threshold density of 169 W/cm^2. The characteristic temperatures, T_0 and T_1, between 200K and 300K were 119K and 171K, respectively. However, these high

performance lasers were not achieved on larger lattice constant buffers. This loss of performance is primarily due to SRH recombination as determined by PL measurements. Low defect, virtual substrates improve the performance of mid-IR lasers. The ultimate degradation of the metamorphic buffers may be avoided with the advent of GaInSb substrates with low defect densities.

There are many items that can still be pursued in an effort to improve these structures. The parameter growth space for AlInSb metamorphic buffers is huge. Only a small number of possible metamorphic buffer layers have been pursued. Other buffer configurations can be pursued to promote smoother surfaces in order to reduce scattering losses and to optimize interface strains to improved dislocation filtering. Also, alternatives to metamorphic buffers can be pursued in the form of ternary substrates from bulk crystal growth. Samples grown in this thesis were pure antimonide because of the simplicity of growth. Small amounts of arsenic can be used to substantially increase wavelengths without much loss of valence band offsets in type-I structures. Also, the possibility of type-II structures can be taken advantage of to provide larger gains and larger differential gains on metamorphic buffers as compared to type-II structures grown on GaSb.

List of References

[1] Andrew Ongstad, email, Jan. 2002.

[2] S. A. Miller, Photonics Spectra **July**, 87 (1986).

[3] R. U. Martinelli, Laser Focus World **March**, 77 (1996).

[4] F. Hanson, Optical Engineering **39**, 3044 (2000).

[5] W. T. Tsang and N. A. Olsson, Applied Physics Letters, **43**, 8 (1983).

[6] I. Mengailis, R. J. Phelan, and R. H. Rediker, Applied Physics Letters **5**, 5 (1964).

[7] T. Ashley, C. T. Elliot, R. Jefferies, A. D. Johnson, G. J. Pryce, A. M. White, and M. Carroll, Applied Physics. Letters **70**, 931 (1997).